Effect of Film Thickness on the Phase Behaviors of Diblock Copolymer Thin Film

Jueun Jung,[†] Hae-Woong Park,[†] Sekyung Lee,[†] Hyojoon Lee,[†] Taihyun Chang,[†,*] Kazuyuki Matsunaga,[‡] and Hiroshi Jinnai[‡,§]

[†]Department of Chemistry and Division of Advanced Materials Science, Pohang University of Science and Technology (POSTECH), Pohang 790-784, Korea, [‡]Department of Macromolecular Science and Engineering, Graduate School of Science and Engineering, Kyoto Institute of Technology, Kyoto 606-8585, Japan, and [§]WPI Advanced Institute for Materials Research, Tohoku University, Sendai 980-8577, Japan

ABSTRACT A phase diagram was constructed for a polystyrene-*block*-polyisoprene (PS-*b*-PI, M_W = 32 700, f_{PI} = 0.670) in thin films on Si wafer as a function of film thickness over the range of 150−2410 nm (7−107L_0 (L_0: domain spacing)). The PS-*b*-PI exhibits a variety of ordered phases from hexagonally perforated lamellar (HPL) *via* double gyroid (DG) to hexagonally packed cylinder (HEX) before going to the disordered (DIS) phase upon heating. The morphology of the PS-*b*-PI in thin film was investigated by grazing incidence small-angle X-ray scattering, transmission electron microscopy, and transmission electron microtomography. In thin film, the phase transition temperature is difficult to be determined unequivocally with *in situ* heating processes since the phase transition is slow and two phases coexist over a wide temperature range. Therefore, in an effort to find an "equilibrium" phase, we determined the long-term stable phase formed after cooling the film from the DIS phase to a target temperature and annealing for 24 h at the temperature. The temperature windows of stable ordered phases are strongly influenced by the film thickness. As the film thickness decreases, the temperature window of layer-like structures such as HPL and HEX becomes wider, whereas that of the DG stable region decreases. For the films thinner than 160 nm (8L_0), only the HPL phase was found. In the films exhibiting DG phase, a perforated layer structure at the free surface was found, which gradually converts to the internal DG structure. The relief of interfacial tension by preferential wetting appears to play an important role in controlling the morphology in very thin films.

KEYWORDS: block copolymer · phase diagram · thin film · PS-*b*-PI · grazing incidence X-ray scattering · transmission electron microtomography

Block copolymers self-assemble into various microphase-separated morphologies, and the ordered morphology in nanoscale has attracted much attention due to its potential applications of nanostructured materials or nanotemplates.[1−5] The phase behavior of diblock copolymers in bulk was found to be predictable in terms of the total number of the segment (N), composition (f), and the interaction parameter (χ) of two blocks, and the phase diagrams of diblock copolymers are often constructed in the form of $N\chi$ *vs* f plot.[6−9] Since the χ parameter is a function of temperature, such phase diagrams has been experimentally constructed from the temperature dependent phase behaviors of block copolymers.[10−13]

Most of potential applications of the well-ordered nanoscale pattern obtained from self-assembled block copolymers are in the form of thin film.[14−17] The phase behavior of block copolymers in thin film is known to deviate from the bulk behavior since it is influenced by the interfacial interaction (with substrate and/or free surface) of block components and the confined geometry of thin films. A block interacting preferentially with the substrate surface or free surface wets the corresponding interface and induces preferential orientation of nanodomains as well.[18−23] These effects become more significant as the film thickness decreases[14,24] and diverse ordered nanostructures have been achieved with a better control of orientation than bulk by tuning the film thickness and interfacial interaction.[25−30]

Although a number of studies have reported on block copolymer phase behaviors in thin film including order−order transition (OOT) as well as order−disorder transition (ODT), there are few systematic studies on this important issue. For examples, Arceo *et al*. investigated order−disorder transition temperature (T_{ODT}) in 10−40 nm thick film of symmetric polystyrene-*block*-poly(methylmethacrylate) and found that T_{ODT} of the lamellar (LAM) phase was significantly higher than that of the bulk.[31] Shin *et al*. reported on symmetric polystyrene-*block*-polyisoprene (PS-*b*-PI) that attractive interaction enhanced the orientation of the LAM nanodomain parallel to the film surface even in 40L_0 thickness (L_0: domain spacing) and T_{ODT} increased as the film thickness was decreased.[32] For asymmetric

*Address correspondence to tc@postech.ac.kr.

Received for review February 18, 2010 and accepted May 19, 2010.

Published online May 25, 2010. 10.1021/nn1003309

© 2010 American Chemical Society

TABLE 1. Characteristics of the Thin Films Used in This Study

code[a]	concentration (wt%)[c]	thickness (nm)[d]
$7L_0$	3	150
$8L_0$	3.3	160
$9L_0$	3.5	175
$10L_0$	4	194
$14L_0$	5	310
$34L_0$	10	755
$107L_0$[b]	20	2410

[a]The number stands for the number of layers counted in the HPL phase annealed at 120 °C. [b]The number stands for the number of d$\{121\}_{DG}$ calculated from the domain spacing of $\{121\}_{DG}$ obtained from the GISAXS pattern and film thickness [c]Concentration of the toluene solution spin-coated onto Si wafer. [d]Measured by ellipsometry

diblock copolymers, most studies were concerned with the morphological change in thin film from bulk morphology due to the preferential wetting of a block component in the confined geometry.[33−38] Recently, Shin *et al*. reported on the thermal phase transition behavior of an asymmetric PS-*b*-PI in thin film relative to bulk.[39] The PS-*b*-PI (f_{PI} = 0.667) shows a phase transition pathway in bulk from LAM, hexagonally perforated layer (HPL), double gyroid (DG), hexagonally packed cylinder (HEX) to disordered (DIS) phase upon heating. In the 960 nm thick film on Si wafer, phase behavior was changed greatly. T_{OOT} values of LAM → HPL and HPL→DG increased significantly (~30 °C), and the DG phase was converted to the DIS phase bypassing HEX phase at a T_{ODT} a little higher than that of bulk.

In this study, we carried out a more systematic investigation on the thermal phase behavior of an asymmetric PS-*b*-PI thin film on Si wafer to construct a phase diagram as a function of film thickness and temperature. For the morphology characterization, grazing incidence X-ray scattering (GISAXS) and transmission electron microtomography (TEMT) were used as the major tools.[19,40−43]

RESULTS AND DISCUSSION

The film thickness effect on thermal phase behaviors of PS-*b*-PI thin film was investigated over the thickness range of 150−2410 nm. In Table 1 are listed the thickness and the concentration of toluene solution spin-coated for the PS-*b*-PI thin films used in this study. The sample codes of the thin films stand for the thickness of the film in terms of the number of layers counted in the TEM image of the HPL phase annealed at 120 °C except for the $107L_0$ sample. ($L_0 \approx 23$ nm). In the case of $107L_0$, which does not show a HPL phase, the number of domains was calculated from the domain spacing of $\{121\}_{DG}$ obtained from the GISAXS pattern and the film thickness.

***In-Situ* Heating Measurements.** In general, the phase transition of block copolymers is retarded in thin film due to the interaction between the wetting block and the substrate surface.[44] Since the retarded kinetics can complicates the analysis of the phase behavior in thin film we first examined the problems associated with the retarded kinetics. Figure 1 shows the representative GISAXS patterns of the various morphologies observed from the $34L_0$ (755 nm thick) film at different temperatures. The spin-coated film was preannealed at 120 °C for 24 h and the GISAXS pattern was monitored as the sample was heated from 120 to 260 °C at a rate of 2 °C/min. The HPL (a) phase first developed from 120 °C was converted to DG (b), HEX (c), and DIS in sequence upon heating. The GISAXS patterns correspond to the ordered phases whose $\{003\}_{HPL}$, $\{121\}_{DG}$, $\{10\}_{HEX}$ are orientated parallel to the substrate plane, respectively, and the pattern of HPL phase (a) corresponds to the ABC stacking of the perforations.[19−21,45]

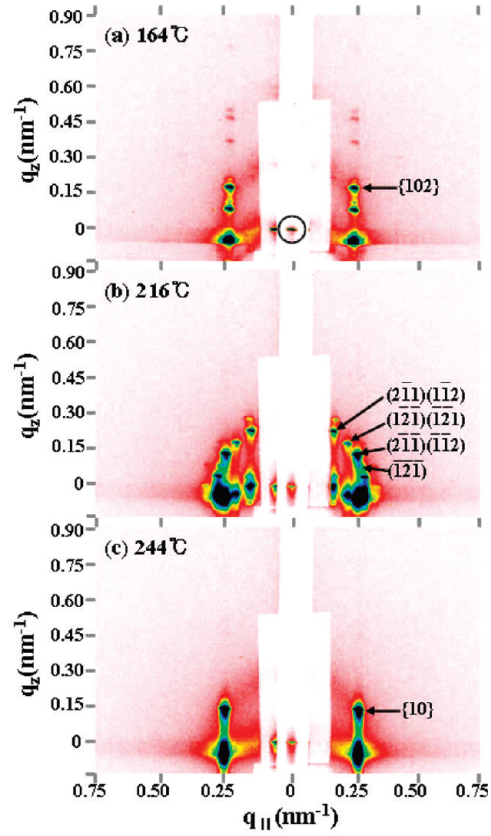

Figure 1. The GISAXS patterns of $34L_0$ obtained during heating at a rate of 2 °C/min from 120 to 260 °C. The circle in panel a indicates the position of the X-ray beam reflected from the silicon wafer. The GISAXS patterns obtained at different temperatures are from the (a) HPL, (b) DG, and (c) HEX phase. The marked spots corresponding to $\{102\}_{HPL}$, $\{121\}_{DG}$, and $\{10\}_{HEX}$ are used to determine T_{OOT}.

To determine T_{OOT} and T_{ODT}, we measured the domain spacing ($2\pi/q$) of the $\{003\}_{HPL}$, $\{121\}_{DG}$, and $\{10\}_{HEX}$ planes in the three ordered phases. They are the planes of most dense minor block distribution which interconvert epitaxially one another in the order−order transition.[20,21,41] The spots corresponding to $\{102\}_{HPL}$, $(2\bar{1}1)(1\bar{1}2)_{DG}$, and $\{10\}_{HEX}$ are labeled in Figure 1. Since the $\{003\}_{HPL}$ refection was blocked by a metal strip (to

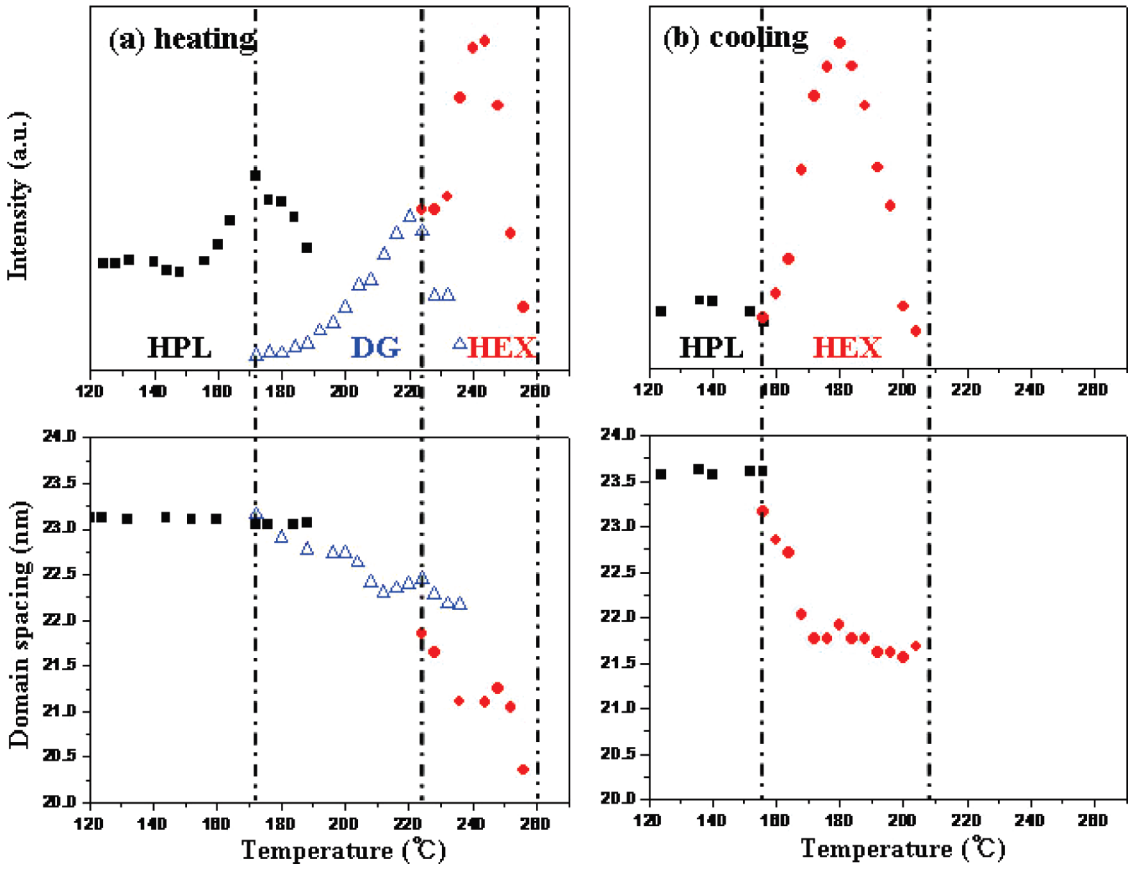

Figure 2. Temperature dependence of intensity (top) and domain spacing (bottom) of the 34L_0 film obtained from GISAXS experiments. They were obtained upon heating (left) and cooling (right) the film at a rate of 2 °C/min. The filled square, open triangle, and filled circle symbols represent the intensity data obtained from $\{102\}_{HPL}$, $(2\bar{1}1)(1\bar{1}2)_{DG}$, and $\{10\}_{HEX}$ reflections shown in Figure 1, respectively. And the domain spacing of $\{003\}_{HPL}$, $\{121\}_{DG}$, and $\{10\}_{HEX}$ planes are calculated from the diffraction angle of the spots.

protect the detector from the intense specular reflection), the domain spacing of $\{003\}_{HPL}$ was obtained indirectly from $\{102\}_{HPL}$ reflection. And the domain spacing of $\{121\}_{DG}$ was calculated from $(2\bar{1}1)(1\bar{1}2)$ spot among the $\{121\}_{DG}$ family spots. The $(2\bar{1}\bar{1})(\bar{1}\bar{1}2)_{DG}$ spot was more intense than $(21\bar{1})(1\bar{1}2)_{DG}$, but it partially overlapped with the peaks from $\{10\}_{HEX}$. In Figure 2, the intensity of $\{102\}_{HPL}$, $\{121\}_{DG}$, $\{10\}_{HEX}$ reflections (labeled in Figure 1) and the domain spacing of $\{003\}_{HPL}$, $\{121\}_{DG}$, and $\{10\}_{HEX}$ planes in the 34L_0 film are plotted as a function of temperature. In this *in situ* experiment, heating and cooling rate was 2 °C/min, which is a typical *in situ* heating rate to construct a phase diagram of block copolymers.[10,13]

Upon heating, the intensity of $\{102\}_{HPL}$ reflection increases as the temperature approaches T_{OOT} to DG phase and then begins to decrease as $\{121\}_{DG}$ reflection appears at 172 °C. The similar behavior is also observed for the phase transition from DG to HEX phase at 224 °C. T_{OOT} is taken as 172 and 224 °C for the HPL → DG and DG → HEX transitions, respectively, at which an abrupt intensity change occurs and a new phase starts to show up. At these transition temperatures, the domain spacings (bottom plot) of $\{003\}_{HPL}/\{121\}_{DG}$ and $\{121\}_{DG}/\{10\}_{HEX}$ nearly match one another at the corresponding phase boundary as confirmed in the previous studies.[20−22] The good match of the domain spacing reflects a good epitaxial manner of the phase transition. The HEX phase is converted to the disordered phase at 260 °C as identified with a complete conversion to a ring-shaped GISAXS pattern. Each phase transition temperature is marked with dash-dot lines in Figure 2. The GISAXS patterns were acquired every 4 °C, and the temperature in the plot indicates the value at which the GISAXS measurements started. Since temperature was changing continuously during the accumulation of the scattering intensity, which took 30 s, some uncertainty in the sample temperature (~1 °C) is unavoidable. Furthermore, the transition to or from DG is not sharp and there is a relatively wide temperature range at which DG coexists with HPL or HEX. It indicates that the transition to or from DG is slow and causes some uncertainly in the determination of the transition temperature.

***In-Situ* Cooling Measurements.** The cooling process (right) shows a much different phase transition behavior from the heating process. T_{ODT} appears at a much lower temperature than that in the heating process. DIS shows up to 208 °C (260 °C in the heating process), and the HEX phase is maintained from 204 to 156 °C. Upon cool-

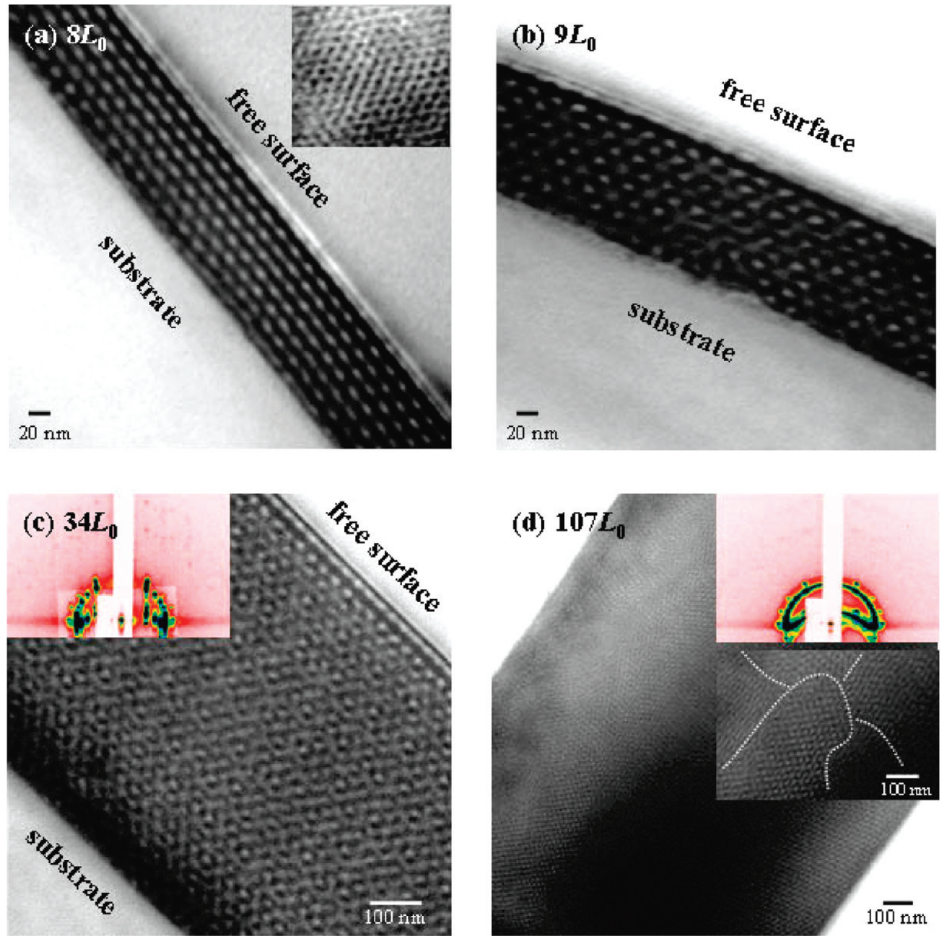

Figure 3. Cross-sectional TEM images of PS-*b*-PI thin films annealed for 1 day, stained with OsO_4: (a) $8L_0$ film (160 nm thick) annealed at 200 °C. The inset is a plan-view showing hexagonal perforation of HPL phase (b) $9L_0$ film (175 nm thick) annealed at 190 °C. (c) $34L_0$ film (755 nm thick) annealed at 180 °C. In the inset, the characteristic GISAXS pattern of DG phase is shown. (d) $107L_0$ film (2.4 μm thick) annealed at 180 °C. $107L_0$ film is too thick to show good orientation of the grains, which is also confirmed by the partially ring-shaped GISAXS pattern in the inset. In the inset, grain boundaries are drawn with dotted lines in an expanded cross-sectional TEM micrograph.

ing, the domain spacing of $\{10\}_{HEX}$ increases to 23.2 nm at 156 °C which is similar to the layer spacing of $\{003\}_{HPL}$, 23.6 nm. Then the HEX phase is transformed to the HPL phase directly bypassing the DG phase. The HEX to HPL transition occurs rapidly, and there is no overlapped region at which characteristic peaks of two ordered phases coexist. These results clearly indicate that the phase transition in thin film is slow, particularly those involving the DG phase. The undercooling behavior of the DG phase is so serious that the DG phase does not show up at all in the cooling process. Upon the heating process, the overheating also affects the presence of the DG phase. At a heating rate of 4 °C/min, the HPL phase is converted to the HEX phase, bypassing the DG phase.

Long-Term Stable Phase. On the basis of the measurements discussed, this type of temperature scan does not seem to be an appropriate method to acquire a reliable phase diagram of block copolymers in thin film. Therefore, in this study, individual film samples were prepared by long-term annealing to find a long-term stable (if not equilibrium) morphology at different temperatures. All films were preannealed above T_{ODT} for 1 h. Then the temperature was changed to a target temperature at ~6 °C/min, and the film was annealed at the target temperature for 24 h. After the annealing, thin films were quenched to room temperature to freeze the morphology developed at the target temperature. Since the films thinner than 160 nm ($8L_0$) showed too weak a GISXAS peak to identify the morphology unambiguously, the morphologies of the thin films were identified by cross-sectional and plan-view TEM micrograph. Figure 3 displays a few representative TEM images and GISAXS patterns of the thin films at 4 different thicknesses.

Figure 3a displays the cross-sectional and plan-view TEM image of the $8L_0$ film annealed at 200 °C. The characteristic perforated layer structure of the cross-sectional image and the hexagonally ordered perforations in the plan view confirm the HPL phase unambiguously. TEM images of $9L_0$ film (b) and $34L_0$ film (c) annealed at 180 and 190 °C, respectively, show the characteristic wagon wheel structure of $\{111\}_{DG}$. At the free surface, a layer-like structure exists, and this interfacial

structure was investigated further by TEMT to be discussed later. The inset of Figure 3c shows the GISAXS pattern characteristic of the DG phase in accordance with the TEM image. In fact, the GISAXS pattern shows higher-order peaks indicating excellent ordering of the DG phase in the $34L_0$ film. In the $107L_0$ (2.4 μm thick) film (d), the DG phase prevails but the ordering of the grains is no longer as good as the thinner films. In Figure 3d inset, the GISAXS pattern shows both discrete reflections and a diffuse ring indicating the $\{121\}_{DG}$ plane oriented parallel to the substrate plane and randomly oriented $\{121\}_{DG}$, respectively. The white dotted lines on the TEM image in Figure 3d inset are drawn for visual aid along the apparent grain boundary of the DG phase.

Phase Diagram in Thin Films. On the basis of the GISAXS and TEM results of the thin films annealed at different temperatures, the phase diagram was constructed as a function of film thickness and temperature as shown in Figure 4. A bulk specimen (about 1 mm thick film) is included in addition to the thin films listed in Table 1. The abscissa is plotted in logarithmic scale to span the wide thickness range of the samples from 150 nm to 1 mm. The four different morphologies observed in this system are denoted with different symbols: HPL (■), DG (Δ), HEX (●) and DIS (◇), respectively. The phase boundaries were drawn by dotted lines for visual aid. The long-term stability of the morphology was examined for two $34L_0$ samples in HPL and DG phase (they are marked with a circle in Figure 4) by annealing for 7 days in vacuum, and no further phase evolution was observed.

First of all, this phase diagram shows a big difference from the transition temperatures observed by *in situ* heating experiments (Figure 2). To show the contrast clearly, the phase windows for the $34L_0$ film observed in the *in situ* heating experiment are drawn on the phase diagram. The T_{OOT} values and T_{ODT} measured by *in situ* heating experiment are much higher (~20 °C or more) than the phase diagram constructed in this study, which indicates the temperature lag in the *in situ* heating experiment due to the slow phase transition kinetics in thin film.

Order−disorder transitions of the PS-*b*-PI occurs at ~205 °C in bulk. As the film thickness decreases, T_{ODT} gradually increases to 250 °C and appears to reach an asymptote around the thickness of 300 nm. The interaction between the polymer and the substrate (and/or air) in thin film must have led to higher T_{ODT} in thin film. The selective interactions between the substrate and a block would enhance the stability of the segregated mesostructure and suppression of compositional fluctuations.[31,32] The preferential wetting of PI block to the free surface is evident as elaborated later.

For the order−order phase transition, three ordered phases of HPL, DG, and HEX appear in the phase diagram. The bulk and $107L_0$ film show a very narrow HEX window just below T_{ODT} followed by a wide DG

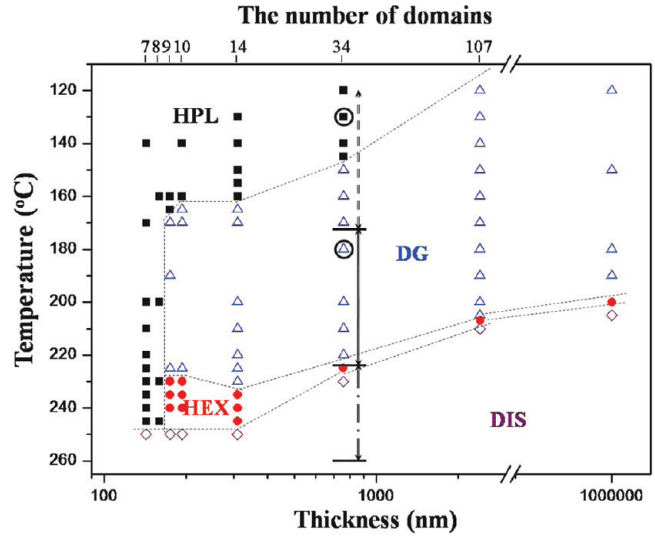

Figure 4. Phase diagram for PS-*b*-PI thin film and bulk as a function of thickness and temperature. For visual aid, the phase boundaries are drawn with dotted lines. Two $34L_0$ samples marked by circles were annealed for 7 days to confirm the long-term stability. The phase transition temperatures measured for $34L_0$ film by *in situ* heating experiments are drawn with lines to compare with the long-term annealing experiment results. Dashed line, solid line, and dash−dot line represent HPL, DG, and HEX stable region, respectively.

phase window and no HPL phase down to 120 °C in the phase diagram. The lowest temperature in the phase diagram was 120 °C since we were concerned that at lower temperature the polymer chain mobility might become too low to establish a long-term stable phase in 24 h annealing as it approached the glass transition temperature of PS. As the film becomes thinner, the HPL phase starts to show up in the phase diagram and the temperature window of the HPL phase increases up to 160 °C at the $14L_0$ film. The HEX window is also broadened a little so that the DG stable temperature range shrinks to a temperature range between 170 and 225 °C for the $9L_0$ film. For the films thinner than $9L_0$, the DG stable region disappears and only the HPL phase is observed. Therefore, at least a thickness of $9L_0$ seems to be necessary to develop the DG phase in this system. In contrast, the HPL (and HEX to some extent) phase has a layer structure with its orientation parallel to the interfacial plane in the thin films which can minimize interfacial energy effectively.

Structure at the Free Surface. As displayed in Figure 3b,c, the DG phase shows a layer structure at the free surface indicating that the 3D network structure is not maintained to the free surface. It could be a reason why the DG structure is no longer stable in very thin films. The surface structure of thin films was further investigated in detail using TEMT. Figure 5 shows digitally sliced images and a 3D image of the $34L_0$ film annealed at 180 °C for 1 day. Figure 5a is a cross-sectional image across the film thickness. The sliced image shows a clear $\{111\}_{DG}$ plane with near perfect orientation of $\{121\}_{DG}$ parallel to the film plane ($x-z$ plane).

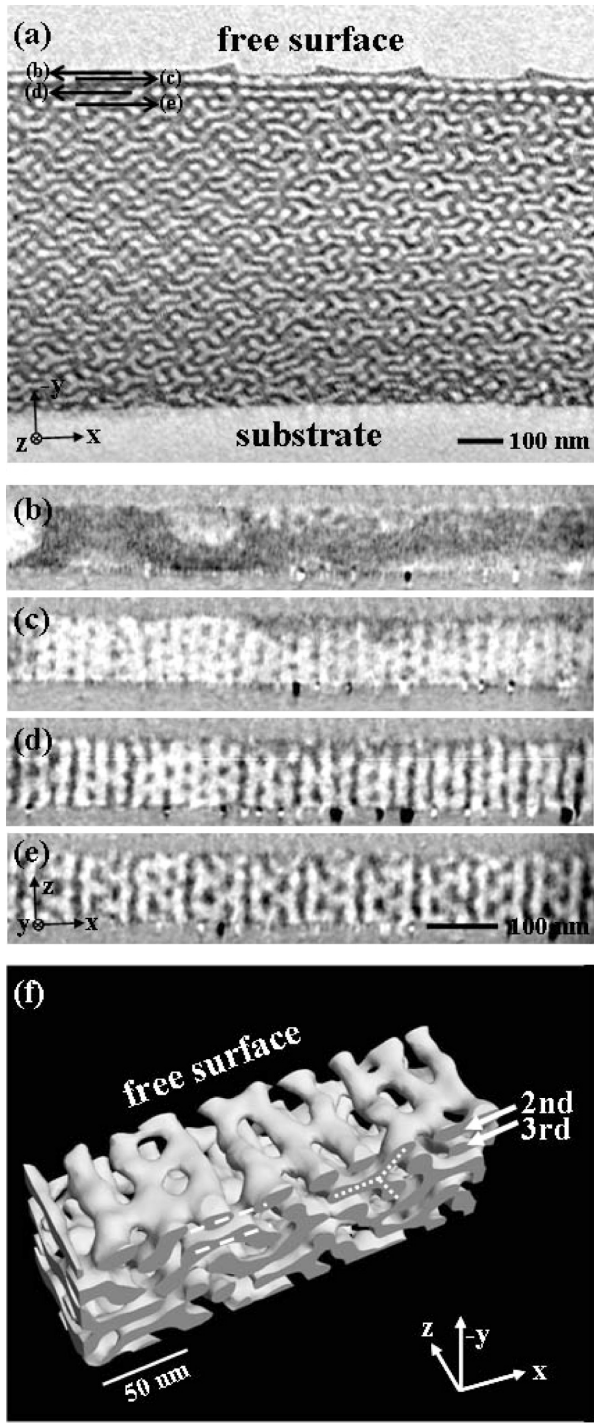

Figure 5. (a) Digitally sliced cross-sectional view across the film thickness. The *x*−*z* plane is parallel to the substrate. (b−e) Digitally sliced plan views near the free surface at different depths from the surface PI layer (b), the first PS-rich layer (c), the second PS-rich layer (d), and the third PS-rich layer (e). Each layers corresponding to panels b−e are marked with an arrow in panel a. (f) 3D image near the free surface showing the second PS-rich layer to the fifth PS-rich layer.

Since the interfacial energy of PI is lower than PS at both interfaces with the substrate (Si wafer) and free surface (vacuum), PI is supposed to wet both interfaces.[46,47] As expected, the surface layer at the free surface is a PI layer appearing dark in Figure 5b. It is partially damaged during the TEM sampling process. The next (the first PS-rich) layer shown in Figure 5c is perforated like the HPL phase. The second and third PS-rich layers (Figure 5d,e) exhibit a progressive change from the HPL-like layer to the DG structure as it goes deeper into the film. The second PS-rich layer shown in Figure 5d shows a transition to the DG phase, and the characteristic $\{121\}_{DG}$ structure becomes apparent at the third PS-rich layer as shown in Figure 5e. Figure 5f displays the 3D image of the specimen from the second PS-rich layer to the fifth PS-rich layer. Only the PS domain is shown for visual clarity. A part of the second layer is fully separated from the third layer as in the HPL phase (dashed line), while the other part is 3-dimensionally linked by a tripod skeleton as in the DG phase (dotted line). This transient structure is different from the coexisting phase of HPL and DG found in the HPL → DG phase transition,[21,48] in which $\{003\}_{HPL}$ and $\{121\}_{DG}$ are connected by edge and do not show an intermediate layer structure. Although surface structure perturbation of asymmetric diblock copolymer in thin film has been reported previously,[23,38] it is demonstrated unambiguously by TEMT images in this study. The surface structure was found to be so stable that it remained unchanged after the annealing for 3 days. Such high stability of the interfacial structure should be a result of the forced progressive transition starting from the PI wetting layer. The transition from perforated layer structure like HPL to the neat DG structure takes place over 3−4 layers. This seems to be the major reason why the DG stable region diminishes as the film thickness decreases in the phase diagram shown in Figure 4. Precise observation of the wetting layer at the substrate was not possible since it was damaged during the detachment process of the film from the substrate. Nonetheless, such a layer-like structure found at free surface is not evident at the interface with the Si substrate as can be seen in Figure 5a. The silicon oxide surface appears not to be as selective as the free surface in differentiating the PS and PI blocks.

In summary, we investigated the phase behavior of PS-*b*-PI thin films as a function of the film thickness. In thin film, the phase transition becomes slower and the hysteresis in the thermal phase transition behavior gets more serious, in particular for the DG phase. The conversion of DG phase from or to other ordered phases occurs slowly. It is sometimes bypassed at a fast heating or cooling rate. Therefore, instead of *in situ* heating or cooling experiments, we tried to achieve a long-term stable, if not equilibrium, phase at different temperatures. On the basis of the block copolymer morphology in thin films annealed for 24 h, we constructed a phase diagram of PS-*b*-PI thin films on Si wafer in the thickness range of 150−2410 nm and bulk as a function of film thickness and temperature. T_{ODT} in thin film increases as the film thickness decreases down to ~300 nm ($14L_0$) and reached an asymptote at ~45 °C higher than that

in bulk. The temperature regions of the stable ordered phases were strongly influenced by the film thickness. Upon decreasing the film thickness, HPL and HEX that are layer-like structures showed up over a broader temperature window, whereas the DG phase showed an opposite tendency. For the films thinner than 160 nm ($8L_0$), we observed HPL phase only. From TEMT results, the thin films in the DG phase were found to exhibit a progressive change from the PI wetting layer, *via* perforated PS layer, to the internal DG phase at the free surface. The structural transition takes place over $3-4L_0$ thickness, and it seems to be a major reason of the instability of the DG phase which expands the HPL window in very thin films.

EXPERIMENTAL DETAILS

The PS-*b*-PI was synthesized *via* sequential anionic polymerization and characterized by size exclusion chromatography coupled with light scattering detection (Wyatt, WTREOS-05) and ^{1}H NMR (Bruker, DPX-300).[49,50] The number average molecular weight (M_n), the polydispersity index (M_w/M_n) and the volume fraction of PI (f_{PI}) were found to be 32 300, 1.01, and 0.670, respectively.

To investigate the effect of film thickness, seven thin films of different thickness were prepared via spin coating of 3−20 wt % toluene solution at 2000 rpm onto silicon wafers with ~500 nm oxide layer. The silicon wafer was cleaned in piranha solution prior to spin coating. A small amount (<1 wt %) of antioxidant (Irganox 1010) was added in the toluene solutions to protect the PI block from thermal degradation. The thickness of thin films was measured by an ellipsometer (J.A. Woollam Co., Inc., EC-400).

After the spin-coating, the films were vacuum-dried at room temperature for 1 h to remove residual solvent. After drying, the films were annealed in vacuum at ~10 °C higher than the T_{ODT} for 1 h to erase initial memory completely, and then they were cooled down (~6 °C/min) to a target temperature. The films were then annealed at the target temperature for 1 day to develop the "equilibrium" phase. After the annealing, the films were quenched to room temperature rapidly over a few seconds to freeze the morphology developed at the annealing temperature using a homemade vacuum oven that was designed to cool down the polymer thin film samples quickly.[41]

The morphology of PS-*b*-PI thin films was examined by GISAXS, TEM, and TEMT. The GISAXS experiment was performed at the 4C2 beamline of the Pohang Accelerator Laboratory, Pohang, Korea.[19] The wavelength (λ) of the X-ray beam was 1.54 Å´. The critical angles of the silicon wafer and the polymer film were calculated from the electron density as 0.22° and 0.15°, respectively, and the incident angle was set at 0.18−0.20°. The sample-to-detector distance was 2.2 m. The exposure time for the GISAXS experiments was 15−60 s. After the GISAXS experiments, the polymer films were detached from Si wafer using 3 vol% aqueous HF solution for TEM and TEMT measurement. The polymer films were embedded in epoxy resin and microtomed (RMC Ultracut) to the cross-sectional thickness of ~100 nm before transferring to C-coated or polyvinylformal-coated Cu grids. Details of the sampling method were reported elsewhere.[21,41] Before taking an image, the PI block was stained with OsO_4 (Polysciences, 0.4% in water) for 20 min. TEM (Hitachi-7600) was operated at 80 kV in bright field. TEMT measurements were performed on JEM-2200FS (JEOL Co., Ltd., Japan) at an accelerating voltage of 200 kV.[51] The TEM micrographs were obtained at 1° increment between −65° and +65° tilt angle. The image set was processed according to the same protocol described elsewhere.[42]

Acknowledgment. T.C. acknowledges the supports from NRF *via* NRL (R0A-2007-000-20125-0), SRC (R11-2008-052-03002) and WCU (R31-2008-000-10059-0) programs. H.J. is grateful for support from the Ministry of Education, Science, Sports and Culture through Grant-in-Aid No. 2101517. The GISAXS measurements at PAL were supported by the Ministry of Science and Technology and POSCO.

REFERENCES AND NOTES

1. Glass, R.; Moller, M.; Spatz, J. P. Block Copolymer Micelle Nanolithography. *Nanotechnology* **2003**, *14*, 1153–1160.
2. Hamley, I. W. Nanostructure Fabrication Using Block Copolymers. *Nanotechnology* **2003**, *14*, R39–R54.
3. Crossland, E. J. W.; Kamperman, M.; Nedelcu, M.; Ducati, C.; Wiesner, U.; Smilgies, D. M.; Toombes, G. E. S.; Hillmyer, M. A.; Ludwigs, S.; Steiner, U.; Snaith, H. J. A Bicontinuous Double Gyroid Hybrid Solar Cell. *Nano Lett.* **2009**, *9*, 2807–2812.
4. Park, H. J.; Kang, M. G.; Guo, L. J. Large Area High Density Sub-20 nm SiO_2 Nanostructures Fabricated by Block Copolymer Template for Nanoimprint Lithography. *ACS Nano* **2009**, *3*, 2601–2608.
5. Zhao, Y.; Thorkelsson, K.; Mastroianni, A. J.; Schilling, T.; Luther, J. M.; Rancatore, B. J.; Matsunaga, K.; Jinnai, H.; Wu, Y.; Poulsen, D.; *et al*. Small-Molecule-Directed Nanoparticle Assembly Towards Stimuli-Responsive Nanocomposites. *Nat. Mater.* **2009**, *8*, 979–985.
6. Leibler, L. Theory of Microphase Separation in Block Copolymers. *Macromolecules* **1980**, *13*, 1602.
7. Bates, F. S.; Fredrickson, G. H. Block Copolymer Thermodynamics: Theory and Experiment Annu. *Rev. Phy. Chem.* **1990**, *41*, 525–557.
8. Matsen, M. W.; Bates, F. S. Unifying Weak- and Strong-Segregation Block Copolymer Theories. *Macromolecules* **1996**, *29*, 1091–1098.
9. Cochran, E. W.; Garcia-Cervera, C. J.; Fredrickson, G. H. Stability of the Gyroid Phase in Diblock Copolymers at Strong Segregation. *Macromolecules* **2006**, *39*, 2449–2451.
10. Khandpur, A. K.; Forster, S.; Bates, F. S.; Hamley, I. W.; Ryan, A. J.; Bras, W.; Almdal, K.; Mortensen, K. Polyisoprene−Polystyrene Diblock Copolymer Phase Diagram near the Order−Disorder Transition. *Macromolecules* **1995**, *28*, 8796–8806.
11. Fischer, H.; Weidisch, R.; Stamm, M.; Budde, H.; Horing, S. The Phase Diagram of the System Poly(styrene-*block*-*n*-butyl methacrylate). *Colloid Polym. Sci.* **2000**, *278*, 1019–1031.
12. Floudas, G.; Vazaiou, B.; Schipper, F.; Ulrich, R.; Wiesner, U.; Iatrou, H.; Hadjichristidis, N. Poly(ethylene oxide-*b*-isoprene) Diblock Copolymer Phase Diagram. *Macromolecules* **2001**, *34*, 2947–2957.
13. Park, S.; Kwon, K.; Cho, D.; Lee, B.; Ree, M.; Chang, T. Phase Diagram Constructed from the HPLC Fractions of a Polystyrene-*b*-polyisoprene Prepared by Anionic Polymerization. *Macromolecules* **2003**, *36*, 4662–4666.
14. Fasolka, M. J.; Mayes, A. M. Block Copolymer Thin Films: Physics and Applications. *Annu. Rev. Mater. Res.* **2001**, *31*, 323–355.
15. Kim, J. K.; Lee, J. I.; Lee, D. H. Self-Assembled Block Copolymers: Bulk to Thin Film. *Macromol. Res.* **2008**, *16*, 267–292.
16. Park, S.; Lee, D. H.; Xu, J.; Kim, B.; Hong, S. W.; Jeong, U.; Xu, T.; Russell, T. P. Macroscopic 10-Terabit-Per-Square-Inch Arrays from Block Copolymers with Lateral Order. *Science* **2009**, *323*, 1030–1033.
17. Hamley, I. W. Ordering in Thin Films of Block Copolymers: Fundamentals to Potential Applications. *Prog. Polym. Sci.* **2009**, *34*, 1161–1210.
18. Matsen, M. W. Thin films of Block Copolymer. *J. Chem. Phys.* **1997**, *106*, 7781–7791.

19. Lee, B.; Park, I.; Yoon, J.; Park, S.; Kim, J.; Kim, K. W.; Chang, T.; Ree, M. Structural Analysis of Block Copolymer Thin Films with Grazing Incidence Small-Angle X-ray Scattering. *Macromolecules* **2005**, *38*, 4311–4323.
20. Park, I.; Lee, B.; Ryu, J.; Im, K.; Yoon, J.; Ree, M.; Chang, T. Epitaxial Phase Transition of Polystyrene-*b*-polyisoprene from Hexagonally Perforated Layer to Gyroid Phase in Thin Film. *Macromolecules* **2005**, *38*, 10532–10536.
21. Park, H. W.; Im, K.; Chung, B.; Ree, M.; Chang, T.; Sawa, K.; Jinnai, H. Direct Observation of HPL and DG Structure in PS-*b*-PI Thin Film by Transmission Electron Microscopy. *Macromolecules* **2007**, *40*, 2603–2605.
22. Park, H. W.; Jung, J.; Chang, T. New Characterization Methods for Block Copolymers and Their Phase Behaviors. *Macromol. Res.* **2009**, *17*, 365–377.
23. Lyakhova, K. S.; Sevink, G. J. A.; Zvelindovsky, A. V.; Horvat, A.; Magerle, R. Role of Dissimilar Interfaces in Thin Films of Cylinder-Forming Block Copolymers. *J. Chem. Phys.* **2004**, *120*, 1127–1137.
24. Olszowka, V.; Tsarkova, L.; Boker, A. 3-Dimensional Control over Lamella Orientation and Order in Thick Block Copolymer Films. *Soft Matter* **2009**, *5*, 812–819.
25. Huang, E.; Russell, T. P.; Harrison, C.; Chaikin, P. M.; Register, R. A.; Hawker, C. J.; Mays, J. Using Surface Active Random Copolymers to Control the Domain Orientation in Diblock Copolymer Thin Films. *Macromolecules* **1998**, *31*, 7641–7650.
26. Xu, T.; Hawker, C. J.; Russell, T. P. Interfacial Interaction Dependence of Microdomain Orientation in Diblock Copolymer Thin Films. *Macromolecules* **2005**, *38*, 2802–2805.
27. Ryu, D. Y.; Wang, J. Y.; Lavery, K. A.; Drockenmuller, E.; Satija, S. K.; Hawker, C. J.; Russell, T. P. Surface Modification with Cross-Linked Random Copolymers: Minimum Effective Thickness. *Macromolecules* **2007**, *40*, 4296–4300.
28. Ham, S.; Shin, C.; Kim, E.; Ryu, D. Y.; Jeong, U.; Russell, T. P.; Hawker, C. J. Microdomain Orientation of PS-*b*-PMMA by Controlled Interfacial Interactions. *Macromolecules* **2008**, *41*, 6431–6437.
29. Albert, J. N. L.; Baney, M. J.; Stafford, C. M.; Kelly, J. Y.; Epps, T. H. Generation of Monolayer Gradients in Surface Energy and Surface Chemistry for Block Copolymer Thin Film Studies. *ACS Nano* **2009**, *3*, 3977–3986.
30. Ramanathan, M.; Nettleton, E.; Darling, S. B. Simple Orientational Control over Cylindrical Organic-Inorganic Block Copolymer Domains for Etch Mask Applications. *Thin Solid Films* **2009**, *517*, 4474–4478.
31. Arceo, A.; Green, P. F. Ordering Transition of Block Copolymer Films. *J. Phys. Chem. B* **2005**, *109*, 6958–6962.
32. Shin, C.; Ahn, H.; Kim, E.; Ryu, D. Y.; Huh, J.; Kim, K. W.; Russell, T. P. Transition Behavior of Block Copolymer Thin Films on Preferential Surfaces. *Macromolecules* **2008**, *41*, 9140–9145.
33. Knoll, A.; Horvat, A.; Lyakhova, K. S.; Krausch, G.; Sevink, G. J. A.; Zvelindovsky, A. V.; Magerle, R. Phase Behavior in Thin Films of Cylinder-Forming Block Copolymers. *Phys. Rev. Lett.* **2002**, *89*, 035501.
34. Park, I.; Park, S.; Park, H. W.; Chang, T.; Yang, H. C.; Ryu, C. Y. Unexpected Hexagonally Perforated Layer Morphology of PS-*b*-PMMA Block Copolymer in Supported Thin Film. *Macromolecules* **2006**, *39*, 315–318.
35. Tsarkova, L.; Knoll, A.; Krausch, G.; Magerle, R. Substrate-Induced Phase Transitions in Thin Films of Cylinder-Forming Diblock Copolymer Melts. *Macromolecules* **2006**, *39*, 3608–3615.
36. Heckmann, M.; Drossel, B. Cylindrical Phase of Block Copolymers in Thin Films. *Macromolecules* **2008**, *41*, 7679–7686.
37. Niihara, K. I.; Sugimori, H.; Matsuwaki, U.; Hirato, F.; Morita, H.; Doi, M.; Masunaga, H.; Sasaki, S.; Jinnai, H. A Transition from Cylindrical to Spherical Morphology in Diblock Copolymer Thin Films. *Macromolecules* **2008**, *41*, 9318–9325.
38. Zhang, X. H.; Berry, B. C.; Yager, K. G.; Kim, S.; Jones, R. L.; Satija, S.; Pickel, D. L.; Douglas, J. F.; Karim, A. Surface Morphology Diagram for Cylinder-Forming Block Copolymer Thin Films. *ACS Nano* **2008**, *2*, 2331–2341.
39. Shin, C.; Ryu, D. Y.; Huh, J.; Kim, J. H.; Kim, K. W. Order-to-Order Transitions of Block Copolymer in Film Geometry. *Macromolecules* **2009**, *42*, 2157–2160.
40. Jinnai, H.; Nishikawa, Y.; Spontak, R. J.; Smith, S. D.; Agard, D. A.; Hashimoto, T. Direct Measurement of Interfacial Curvature Distributions in a Bicontinuous Block Copolymer Morphology. *Phys. Rev. Lett.* **2000**, *84*, 518–521.
41. Park, H. W.; Jung, J.; Chang, T.; Matsunaga, K.; Jinnai, H. New Epitaxial Phase Transition between DG and HEX in PS-*b*-PI. *J. Am. Chem. Soc.* **2009**, *131*, 46–47.
42. Jinnai, H.; Spontak, R. J. Transmission Electron Microtomography in Polymer Research. *Polymer* **2009**, *50*, 1067–1087.
43. Jinnai, H.; Spontak, R. J.; Nishi, T. Transmission Electron Microtomography and Polymer Nanostructures. *Macromolecules* **2010**, *43*, 1675–1688.
44. Sohn, B. H.; Seo, B. W.; Yoo, S. I.; Zin, W. C. Sluggish Development of Parallel Lamellae at the Strongly Interacting Interface in Thin Films of Symmetric Diblock Copolymers. *Langmuir* **2002**, *18*, 10505–10508.
45. Heo, K. Y.; Yoon, J. W.; Jin, S. W.; Kim, J. H.; Kim, K. W.; Shin, T. J.; Chung, B. H.; Chang, T. Y.; Ree, M. H. Polystyrene-*b*-polyisoprene Thin Films with Hexagonally Perforated Layer Structure: Quantitative Grazing-Incidence X-ray Scattering Analysis. *J. Appl. Crystallogr.* **2008**, *41*, 281–291.
46. Hasegawa, H.; Hashimoto, T. Morphology of Block Polymers near a Free Surface. *Macromolecules* **1985**, *18*, 589–590.
47. Collins, S.; Hamley, I. W.; Mykhaylyk, T. An Atomic Force Microscopy Study of Ozone Etching of a Polystyrene/Polyisoprene Block Copolymer. *Polymer* **2003**, *44*, 2403–2410.
48. Mareau, V. H.; Akasaka, S.; Osaka, T.; Hasegawa, H. Direct Visualization of the Perforated Layer/Gyroid Grain Boundary in a Polystyrene-*block*-polyisoprene/Polystyrene Blend by Electron Tomography. *Macromolecules* **2007**, *40*, 9032–9039.
49. Kwon, K.; Lee, W.; Cho, D.; Chang, T. Apparatus for Anionic Polymerization under Inert Gas and Polymerization of Polystyrene. *Korea Polym. J.* **1999**, *7*, 321–324.
50. Lee, W.; Cho, D. Y.; Chang, T. Y.; Hanley, K. J.; Lodge, T. P. Characterization of Polystyrene-*b*-polyisoprene Diblock Copolymers by Liquid Chromatography at the Chromatographic Critical Condition. *Macromolecules* **2001**, *34*, 2353–2358.
51. Sugimori, H.; Nishi, T.; Jinnai, H. Dual-Axis Electron Tomography for Three-Dimensional Observations of Polymeric Nanostructures. *Macromolecules* **2005**, *38*, 10226–10233.